Available online at www.sciencedirect.com
SCIENCE DIRECT®
Journal of Computational Physics 192 (2003) 211–230
JOURNAL OF COMPUTATIONAL PHYSICS
www.elsevier.com/locate/jcp

Analyzing radiation diffusion using time-dependent sensitivity-based techniques

Steven L. Lee [a,*], Carol S. Woodward [a], Frank Graziani [a,b]

[a] *Center for Applied Scientific Computing, Lawrence Livermore National Laboratory, P.O. Box 808, Livermore, CA 94551, USA*
[b] *B-Division, Lawrence Livermore National Laboratory, P.O. Box 808, Livermore, CA 94551, USA*

Received 24 March 2003; received in revised form 7 July 2003; accepted 10 July 2003

Abstract

In this paper, we discuss the computation and use of solution sensitivities for analyzing radiation diffusion problems and the dependence of solutions on input parameters. The derivation of the sensitivity equations is given, along with a description of the method for solving them in tandem with the simulation. The parameter values express material opacity as a power-law of material temperature and density. The computed sensitivities reveal important qualitative details about the temperature coupling and diffusion processes. It is also shown that these sensitivities are valuable for ranking the parameters from most to least influential, designing improved experiments, and quantifying uncertainty in the simulation results. Lastly, the numerical examples show that these various types of sensitivity analysis are only moderately expensive to perform relative to solving the simulation by itself.

Keywords: Sensitivity analysis; Opacities; Radiation diffusion

1. Introduction

The computer has become the virtual laboratory. In recent years, the rapid growth in computer memory and speed has meant that multiphysics complex physical systems operating in two and three dimensions can be simulated, analyzed and quantitative information extracted. The need to quantitatively predict physical phenomena means that the sensitivity of our answers to uncertainties in the parameters making up physical models used in simulations must be made known. Otherwise, comparisons between simulation and experiment are of reduced value.

Simulations of astrophysical and inertial confinement fusion (ICF) phenomena are good examples of areas where computer simulations are relied on for virtual experimentation [1–3]. Both areas involve multiple physics models (hydrodynamics, radiation transport, thermonuclear burn) which depend on such

* Corresponding author. Tel.: +925-424-5989; fax: +925-422-6287.
E-mail addresses: slee@llnl.gov (S.L. Lee), cswoodward@llnl.gov (C.S. Woodward), graziani1@llnl.gov (F. Graziani).

0021-9991/$ - see front matter
doi:10.1016/j.jcp.2003.07.031

quantities as equations of state, thermonuclear reaction rates, and opacities. Due to the nature of the equations involved, the various physics processes tend to couple to each other nonlinearly. Hence, uncertainty in a parameter in one physics model can affect other physics models in sometimes unexpected ways. Before we can tackle the sensitivity of solutions in the multiphysics context, however, it is important to understand solution sensitivity for an isolated physics model. Of particular interest in this paper is radiation diffusion.

In radiation diffusion, one area of concern is the understanding of temperature and density dependencies within opacity values. In particular, the opacity tends to be a rather strong function of temperature in grey radiation diffusion. The calculation of opacities has given rise to sophisticated codes that compute the detailed many-body physics of plasmas [4–6]. These codes have, in turn, given rise to opacity databases. For our purposes, we will consider opacity as a parameterized function of material temperature and density. One of the main objectives then is to quantify the sensitivity of our radiation calculations with respect to parameters used to characterize the dependencies of opacity on material density and temperatures.

A common method of computing solution sensitivities is to run a simulation code for many values of the uncertain parameter and then difference the resulting solutions. The technique used is a finite difference method for computing sensitivities and can be inaccurate unless many runs of the simulation code are included. The method is time-consuming, especially for codes that require extensive run time for their solution. An alternative method is to formulate an equation for the solution sensitivities and evolve that equation along with the original physical system. The resulting method simultaneously gives the solution and its sensitivity, requiring a single run of the simulation code. The run time for this method is longer than for the simulation alone, but gives much more information.

In this work, the sensitivities are evolved in time along with the solution. Since sensitivities are defined as the first derivative of the solution with respect to the model parameter, we can develop an equation for the sensitivities by simply differentiating the original model problem with respect to the parameter. This is done for each parameter that we study. Previous work in the area of linear Boltzmann transport has shown that this method of doing sensitivity analysis can lead to accurate estimates of uncertainties in much faster times than a sampling approach [7]. Previous work has also showed that sensitivities can be evolved in time to effectively give solution sensitivities for equations similar to those governing radiation diffusion [8–11].

In this work, we show how this approach is formulated and we demonstrate the application and versatility of carrying out sensitivity analysis experiments on radiation diffusion problems. To illustrate the method with little sacrifice of reality, we have opted to choose an analytic representation for the opacity. We show how sensitivities are calculated and used to determine the most critical parameters for different materials. In addition, we show how sensitivities can be used to make an estimate of the solution error due to uncertainty in the opacity parameters. The cost of these methods varies from problem to problem, but it has been a modest multiple of the time it takes for a solution-only calculation.

An important aspect of doing sensitivity analysis as we present in this paper is that the calculations of sensitivities require opacities to be handled in a fully implicit manner. Fully implicit methods for radiation diffusion have been a very active area of research recently. Solution techniques for fully implicit methods have been developed for both multigroup and grey formulations [12–17]. These methods have been shown to produce very accurate solutions faster than semi-implicit methods on problems in one, two, and three dimensions as well as in parallel [18–20]. With these advances, the opportunity to compute sensitivities for radiation diffusion problems can easily be realized.

An outline of this paper is as follows. In Section 2, we describe our general model for radiation diffusion and in Section 3, we describe our numerical approach to computing solutions and sensitivities. In Section 4, the details of the model problems are described. In Section 5, we give our numerical results, and in Section 6, we describe how our sensitivity computations can be used to gain further insight into the solutions we compute. Lastly, Section 7 gives our conclusions.

2. Flux-limited radiation diffusion model

We consider a sensitivity analysis of the flux-limited grey radiation diffusion equation given by [3,21]

$$\frac{\partial E_{\mathrm{R}}}{\partial t} = \nabla \cdot \left(\frac{c}{3\rho\kappa_{\mathrm{R}}(T_{\mathrm{R}}) + \frac{\|\nabla E_{\mathrm{R}}\|}{E_{\mathrm{R}}}} \nabla E_{\mathrm{R}} \right) + c\rho\kappa_{\mathrm{P}}(T_{\mathrm{M}}) \cdot \left(aT_{\mathrm{M}}^4 - E_{\mathrm{R}} \right), \tag{1}$$

where $E_{\mathrm{R}}(\mathbf{x}, t)$ is the radiation energy density ($\mathbf{x} = (x, y, z)$), $T_{\mathrm{M}}(\mathbf{x}, t)$ is the material temperature, $\rho(\mathbf{x})$ is the material density, c is the speed of light, and $a = 4\sigma/c$ where σ is the Stephan–Boltzmann constant. In the limiter, the norm $\|\cdot\|$ is just the l^2 norm of the gradient vector. The Rosseland opacity, κ_{R}, is a nonlinear function of the density and the radiation temperature, T_{R}, which is defined by the relation $E_{\mathrm{R}} = aT_{\mathrm{R}}^4$. The Planck opacity, κ_{P}, is a nonlinear function of density and material temperature, T_{M}, which is related to the material energy through an equation of state, $E_{\mathrm{M}} = \mathrm{EOS}(T_{\mathrm{M}})$.

Eq. (1) is coupled to an equation expressing conservation of material energy given by

$$\frac{\partial E_{\mathrm{M}}}{\partial t} = -c\rho\kappa_{\mathrm{P}}(T_{\mathrm{M}}) \cdot \left(aT_{\mathrm{M}}^4 - E_{\mathrm{R}} \right). \tag{2}$$

We consider Dirichlet and Neumann boundary conditions for system (1), (2), and we apply appropriate initial conditions, $E_{\mathrm{R}}|_{t=0} = a(T_{\mathrm{R}}|_{t=0})^4$ and $E_{\mathrm{M}}|_{t=0} = \mathrm{EOS}(T_{\mathrm{M}}|_{t=0})$.

As discussed in [22,23], the Rosseland and Planck opacities are taken to be parameterized functions of temperature and density given by

$$\kappa(T, \rho) = bT^{\mu}\rho^{\lambda}. \tag{3}$$

Although [22,23] give specific values of b, μ, and λ for a number of materials, experimental error usually makes the precise values of these parameters difficult to quantify, giving rise to uncertainty in the solution of the diffusion equations. In this paper, we describe a method for calculating sensitivities of the solutions to the three parameters given in (3). These sensitivities can then be used to evaluate the relative importance of the parameters as well as estimate error in the solution energies and temperatures due to small uncertainties in parameter values.

3. Solution and sensitivity methods

In this section, we discuss the solution and sensitivity methods employed for the system given in (1) and (2). We first show how we discretize the system in space, then discuss our use of ordinary differential equation (ODE) time integration techniques and solvers. Lastly, we show how the solution method is easily extended to compute sensitivities.

3.1. Discretization

For spatial discretization, we employ a cell-centered finite difference approach. We use a tensor product grid with N_x, N_y, and N_z cells in the x, y, and z directions, respectively. Defining $E_{\mathrm{R},i,j,k}(t) \approx E_{\mathrm{R}}(\mathbf{x}_{i,j,k}, t)$ and $E_{\mathrm{M},i,j,k}(t) \approx E_{\mathrm{M}}(\mathbf{x}_{i,j,k}, t)$, with $\mathbf{x}_{i,j,k} = (x_i, y_j, z_k)$, and

$$\mathbf{E}_{\mathrm{R}} \equiv \begin{pmatrix} E_{\mathrm{R},1,1,1} \\ \vdots \\ E_{\mathrm{R},N_x,N_y,N_z} \end{pmatrix} \quad \text{and} \quad \mathbf{E}_{\mathrm{M}} \equiv \begin{pmatrix} E_{\mathrm{M},1,1,1} \\ \vdots \\ E_{\mathrm{M},N_x,N_y,N_z} \end{pmatrix},$$

we can write our discrete equations in terms of a discrete diffusion operator given by

$$\mathbf{L}(\mathbf{E}_{\mathrm{R}}) \equiv \left(L_{1,1,1}(\mathbf{E}_{\mathrm{R}}), \ldots, L_{N_x,N_y,N_z}(\mathbf{E}_{\mathrm{R}})\right)^{\mathrm{T}}, \tag{4}$$

and a local coupling operator given by

$$\mathbf{S}(\mathbf{E}_{\mathrm{R}}, \mathbf{E}_{\mathrm{M}}) \equiv (S_{1,1,1}(\mathbf{E}_{\mathrm{R}}, \mathbf{E}_{\mathrm{M}}), \ldots, S_{N_x,N_y,N_z}(\mathbf{E}_{\mathrm{R}}, \mathbf{E}_{\mathrm{M}}))^{\mathrm{T}}, \tag{5}$$

where

$$L_{i,j,k}(\mathbf{E}_{\mathrm{R}}) = \left(\frac{c}{3\rho_{i+1/2,j,k}\kappa_{\mathrm{R},i+1/2,j,k} + \frac{\|\nabla E_{\mathrm{R}}\|_{i+1/2,j,k}}{E_{\mathrm{R},i+1/2,j,k}}} \frac{E_{\mathrm{R},i+1,j,k} - E_{\mathrm{R},i,j,k}}{\Delta x_{i+1/2,j,k}} - \frac{c}{3\rho_{i-1/2,j,k}\kappa_{\mathrm{R},i-1/2,j,k} + \frac{\|\nabla E_{\mathrm{R}}\|_{i-1/2,j,k}}{E_{\mathrm{R},i-1/2,j,k}}} \frac{E_{\mathrm{R},i,j,k} - E_{\mathrm{R},i-1,j,k}}{\Delta x_{i-1/2,j,k}} \right) \Big/ \Delta x_i + y \text{ and } z \text{ terms}$$

and

$$S_{i,j,k}(E_{\mathrm{R},i,j,k}, E_{\mathrm{M},i,j,k}) = c\rho_{i,j,k}\kappa_{P,i,j,k}\left(aT^4_{\mathrm{M},i,j,k} - E_{\mathrm{R},i,j,k}\right). \tag{7}$$

To approximate the Rosseland opacity $\kappa_{\mathrm{R}}(T_{\mathrm{R}})$ at a cell face $\mathbf{x}_{i+1/2,j,k}$, we first compute the average of the fourth powers of T_{R} at $\mathbf{x}_{i,j,k}$ and $\mathbf{x}_{i+1,j,k}$. The Rosseland opacity is then obtained by evaluating κ_{R} using the fourth root of this average. In the flux-limiter, the norm of the gradient vector is approximated using bi-linear interpolation to get the off-direction components of the two relevant interfaces, and the denominator is obtained using arithmetic averaging.

Thus, our discrete scheme is to find $\mathbf{E}_{\mathrm{R}}(t)$ and $\mathbf{E}_{\mathrm{M}}(t)$ such that

$$\frac{\mathrm{d}\mathbf{E}_{\mathrm{R}}}{\mathrm{d}t} = \mathbf{L}(\mathbf{E}_{\mathrm{R}}) + \mathbf{S}(\mathbf{E}_{\mathrm{R}}, \mathbf{E}_{\mathrm{M}}), \tag{8}$$

$$\frac{\mathrm{d}\mathbf{E}_{\mathrm{M}}}{\mathrm{d}t} = -\mathbf{S}(\mathbf{E}_{\mathrm{R}}, \mathbf{E}_{\mathrm{M}}). \tag{9}$$

We write (8) and (9) as a single system of ODEs by defining the solution vector and nonlinear function as

$$y \equiv \begin{pmatrix} \mathbf{E_R} \\ \mathbf{E_M} \end{pmatrix} \quad \text{and} \quad f \equiv \begin{pmatrix} \mathbf{L}(\mathbf{E}_{\mathrm{R}}) + \mathbf{S}(\mathbf{E}_{\mathrm{R}}, \mathbf{E}_{\mathrm{M}}) \\ -\mathbf{S}(\mathbf{E}_{\mathrm{R}}, \mathbf{E}_{\mathrm{M}}) \end{pmatrix}$$

to obtain the discrete ODE system

$$\frac{\mathrm{d}y}{\mathrm{d}t} = f(t, y). \tag{10}$$

3.2. Solution method

The time integration of the ODE system (10) is accomplished via the parallel ODE solver CVODE [24], a software package written in the C language for the solution of general ODE systems. CVODE uses the backward differentiation formula (BDF) [25,26] methods to perform the time integration. The BDF methods are variable in order and step size and are also implicit. This method results in a coupled, non-linear system of the form

$$y_n = \sum_{j=1}^{q} \alpha_j y_{n-j} + h\beta_0 f(t_n, y_n) \tag{11}$$

that must be solved for the solution, y_n, at the new time, t_n. In this system, q is the order of the BDF method used at that step, β_0 is a coefficient related to the order of the method, and $h = t_n - t_{n-1}$ is the current stepsize. For example, solving the ODE system with the backward Euler method (i.e., the BDF method of order 1), leads to the following nonlinear system:

$$0 = G(y) \equiv y - hf(t_n, y) - y_{n-1} \quad \left(\text{i.e., } \frac{y_n - y_{n-1}}{h} = f(t_n, y_n)\right) \tag{12}$$

that must be solved for $y = y_n$ at each time step. For the solution of the nonlinear systems, we use an inexact Newton–Krylov method with Jacobian-vector products approximated by finite differences of the form

$$G'(y)v \approx \frac{G(y + \theta v) - G(y)}{\theta}, \tag{13}$$

where θ is a scalar. Within the Newton–Krylov paradigm using (13), only the implementation of the nonlinear function is necessary and Jacobian matrix entries need never be formed or stored. Heuristic arguments for the case of systems arising from the implicit integration of ODEs show that $\theta = 1$ works quite well [27] and is the choice used in CVODE. An explicit predictor, $y_{n(0)}$, is used as an initial guess to the nonlinear system (12).

We use the GMRES Krylov iterative solver for solution of the linear Jacobian system at each Newton iteration [28]. Preconditioning is generally essential when using Krylov linear solvers, and we employ a number of techniques including lagging and multigrid [29] within our preconditioning strategy. The solution method presented above has been tested on very large, three-dimensional problems and has been shown to be parallel scalable up to almost 6000 processors. As our focus in on the calculation of solution sensitivities, the specific details of the preconditioning method are not discussed here. We refer the interested reader to the discussion of the Schur complement method in [14].

3.3. Computation of sensitivities

In this paper, we examine the effects on solutions to the radiation diffusion model due to changes in values of the parameters in (3). These effects are measured in sensitivities of the solutions, defined by

$$s_p \equiv \frac{\partial y}{\partial p} = \begin{pmatrix} \frac{\partial E_R}{\partial p} \\ \frac{\partial E_M}{\partial p} \end{pmatrix}, \tag{14}$$

where p is one of the set of parameters, $\{\mu, b, \lambda\}$, and s_p is the expected change in E_R and E_M due to changes in the parameter p. The initial values for s_p are either all zeros (if p occurs only in f), or has nonzeros according to (14) for how the initial values of y depend linearly on p.

We can differentiate system (10) with respect to one of our opacity parameters to get the following system:

$$\frac{\mathrm{d}s_p}{\mathrm{d}t} = \frac{\partial f}{\partial y} s_p + \frac{\partial f}{\partial p}, \tag{15}$$

where $p \in \{\mu, b, \lambda\}$. Eq. (15) is a linear ODE system that is easily solved with the same solution methods as described above for the original problem.

We calculate the solution to these equations with the sensitivity version of CVODE [30]. This software augments the ODE system given in (10) with the linear systems (15) for the sensitivity of the solution with respect to each parameter. Thus, a single ODE system is solved giving the radiation diffusion solution as well as the sensitivities of that solution to each of the opacity parameters.

Letting

$$Y(t) \equiv \begin{pmatrix} y(t) \\ s_\mu(t) \\ s_b(t) \\ s_\lambda(t) \end{pmatrix}, \quad F(t, Y, \mu, b, \lambda) \equiv \begin{pmatrix} f \\ \frac{\partial f}{\partial y} s_\mu + \frac{\partial f}{\partial \mu} \\ \frac{\partial f}{\partial y} s_b + \frac{\partial f}{\partial b} \\ \frac{\partial f}{\partial y} s_\lambda + \frac{\partial f}{\partial \lambda} \end{pmatrix},$$

we have the new ODE system

$$\frac{\mathrm{d}Y}{\mathrm{d}t} = F(t, Y, \mu, b, \lambda).$$

Similar to (12), the backward Euler method yields the nonlinear system

$$0 = G(Y_n) \equiv Y_n - hF(t_n, Y_n, \mu, b, \lambda) - Y_{n-1}. \tag{16}$$

Due to the form of F, the Jacobian matrix $\partial G/\partial Y$ has the lower block triangular structure

$$\frac{\partial G}{\partial Y} = I - h\frac{\partial F}{\partial Y} = \begin{pmatrix} I - h\frac{\partial f}{\partial y} & & & \\ -hJ_\mu & I - h\frac{\partial f}{\partial y} & & \\ -hJ_b & & I - h\frac{\partial f}{\partial y} & \\ -hJ_\lambda & & & I - h\frac{\partial f}{\partial y} \end{pmatrix} \tag{17}$$

with

$$J_\mu = \frac{\partial}{\partial y}\left(\frac{\partial f}{\partial y} s_\mu + \frac{\partial f}{\partial \mu}\right)$$

and so on for J_b and J_λ. Higher-order BDFs also yield Jacobian matrices $\partial G/\partial Y$ with this same lower block triangular structure, and with identical block-diagonal entries of the form $I - h\beta_0(\partial f/\partial y)$. The nonlinear systems $G(Y_n) = 0$ are solved by using the simultaneous corrector method [31], a technique in which the Newton iteration uses the block-diagonal portion of $\partial G/\partial Y$ as the linear system matrix. This results in a decoupling that allows $I - h\beta_0(\partial f/\partial y)$ to be used repeatedly in solving the four linear systems that arise in sequence: one linear system for the Newton correction to the ODE variables; and three other linear systems for the corrections to the three sensitivity vectors. Because all of the Jacobian matrices are identical, the latter systems are solved using the same preconditioner and/or linear system solver that were specified for the original ODE problem.

Given knowledge only of f, computation of the derivatives found in F can be difficult. In this work, we approximate these derivatives with centered finite difference techniques, e.g.,

$$\frac{\partial f}{\partial y} s_\mu + \frac{\partial f}{\partial \mu} \approx \frac{f(t, y + \delta s_\mu, \mu + \delta, b, \lambda) - f(t, y - \delta s_\mu, \mu - \delta, b, \lambda)}{2\delta}.$$

A Taylor series analysis shows that this central difference scheme approximates the sensitivity derivative with $O(\delta^2)$ accuracy. The choice of the differencing parameter is more delicate than in (13) because the scalar δ is used to perturb y and a given parameter simultaneously. Our heuristic for δ is based on several

problem-related features, including machine roundoff error and a weighted norm of the given sensitivity vector. These details and alternative finite difference techniques are described in [30]. One could also use automatic differentiation techniques such as ADIC [32,33] to compute sensitivity derivatives.

The sensitivity version of CVODE chooses time steps for the BDF methods so that accuracy is ensured for both solutions of the radiation diffusion system as well as their sensitivities. As in CVODE, implicit problems are solved at each time step using GMRES, and the same preconditioner is used in solving for the state variables and sensitivity vectors.

3.4. Types of sensitivities

In addition to the energy sensitivities, the radiation and material temperature sensitivities $\partial T_R/\partial p$ and $\partial T_M/\partial p$ can be determined. By differentiating the expressions relating energies and temperatures with respect to an opacity parameter

$$\frac{\partial E_R}{\partial p} = \left(4aT_R^3\right)\frac{\partial T_R}{\partial p}, \tag{18}$$

$$\frac{\partial E_M}{\partial p} = \frac{\partial \mathrm{EOS}(T_M)}{\partial T_M}\frac{\partial T_M}{\partial p}, \tag{19}$$

the temperature sensitivities can be determined using the energies and their sensitivities.

In our analysis work involving temperatures, the temperature sensitivities are often more useful if they are scaled by certain quantities. By scaling these sensitivities, one can create *scaled* and *normalized* sensitivities. One notable property of scaled sensitivities such as

$$\mu\frac{\partial T_R}{\partial \mu} \quad \text{and} \quad \mu\frac{\partial T_M}{\partial \mu}$$

is that they share the same units as the solution quantities T_R and T_M. These sensitivities can then be used in a first-order Taylor series expansion, e.g.,

$$T_R(t,\widetilde{\mu},b,\lambda) \approx T_R(t,\mu,b,\lambda) + \left(\frac{\widetilde{\mu}-\mu}{\mu}\right)\mu\frac{\partial T_R}{\partial \mu}, \tag{20}$$

$$T_M(t,\widetilde{\mu},b,\lambda) \approx T_M(t,\mu,b,\lambda) + \left(\frac{\widetilde{\mu}-\mu}{\mu}\right)\mu\frac{\partial T_M}{\partial \mu}, \tag{21}$$

to give a first-order prediction of solution values due to small relative changes in nominal values of a parameter, such as $(\widetilde{\mu}-\mu)/\mu$. Scaled sensitivities indicate the magnitude and direction of changes in the nominal solution based on a small relative increase in a nominal parameter value.

Normalized sensitivities, e.g.,

$$\eta_R = \left(\mu\frac{\partial T_R}{\partial \mu}\right)\Big/ T_R \quad \text{and} \quad \eta_M = \left(\mu\frac{\partial T_M}{\partial \mu}\right)\Big/ T_M \tag{22}$$

can be used to estimate the relative change in the solution

$$\frac{\partial T_R}{T_R} = \frac{\partial \mu}{\mu}\eta_R \quad \text{and} \quad \frac{\partial T_M}{T_M} = \frac{\partial \mu}{\mu}\eta_M \tag{23}$$

given a relative change in the nominal parameter value, $\partial\mu/\mu$. These sensitivities are dimensionless and are often used to give comparative information about the relative importance of different parameters within a physical system.

3.5. Sensitivity software

In recent years, general use packages have become available to aid in the computation of solution sensitivities using the sensitivity equation method described above.

One such package is CVODES [34] developed at Lawrence Livermore National Laboratory. This package includes capabilities for augmenting an ODE solver with the sensitivity equations as discussed above. The ODE solver is CVODE, a C language rewrite of the VODPK package which evolved from LSODE [35]. The CVODES package is written in a "data structure neutral" manner, meaning that all operations on vectors (the simulation data needed by the package) are done through a set of pre-defined interfaces to the computational kernels. Users can either invoke the serial or parallel default vector kernels or supply their own. As a result, the CVODES package assumes no specific layout or structure to the users' data, and the package is reasonably easy to combine with a pre-existing simulation code (as long as the parameters for sensitivity analysis are handled in an implicit manner). The Livermore group will be releasing sensitivity versions of their C language DAE and nonlinear system solvers soon as part of SUNDIALS (suite of nonlinear and differential/algebraic solvers) [36].

Petzold and others have developed another set of packages for sensitivity analysis of Fortran codes. The package DASPK3.0 [31,37,38] is a Fortran package that solves the augmented system of DAEs and sensitivity equations. This package is also written in a data structure neutral manner as described above and consequently can also be combined with pre-existing simulation codes fairly easily.

Both CVODES and DASPK3.0 have hooks for using automatic differentiation codes for the computation of derivatives in the right-hand side of the sensitivity equations. Automatic differentiation packages use parsing techniques to differentiate computer codes to get mathematical derivatives. Two popular packages for this functionality are ADIFOR [39] and ADIC [32] for Fortran and C language codes, respectively.

4. Model problems

We now consider the development, interpretation, and expense of computing sensitivities in addition to solutions for radiation diffusion problems. For this discussion, we use a suite of test problems based on aluminum and beryllium. The problems are one-dimensional so that we can concentrate on the meaning and expense of sensitivities without undue expense of solutions. We chose the materials aluminum and beryllium because they behave somewhat differently in the regimes we study, and thus they require some differences in interpretation. In addition, we consider both closed and open systems so that, again, we can see some differences in the interpretation of sensitivities. Section 5 will go in depth on the solutions and sensitivities for our problems so that we can demonstrate exactly what sensitivities mean for radiation diffusion systems. Below, we give specific information on the test cases.

The densities used for aluminum and beryllium are 2.70 and 1.85 g cm^{-3}, respectively. The analytical formulas for the equation of state

$$E_{\mathrm{M}} = \frac{p_*}{(\gamma_s - 1)} \rho^{\alpha} T_{\mathrm{M}}^{\beta} \tag{24}$$

and Rosseland mean opacity

$$\kappa_{\mathrm{R}}(T, \rho) = b T^{\mu} \rho^{\lambda} \tag{25}$$

are based on the parameters given in Table 1, and are derived from [22]. For example, the Rosseland mean opacity parameters are straightforward to obtain given that $\rho\kappa_{\mathrm{R}} = l_{\mathrm{R}}^{-1}$, the reciprocal of the Rosseland

Table 1
Parameters for equation of state and Rosseland mean opacity

Parameter	Al	Be
α	0.937	0.9976
β	1.145	1.0042
γ_s	1.43	1.57
p_* ($g^{1-\alpha}$ $cm^{3\alpha-1}$ μs^{-2} $eV^{-\beta}$)	1.99e − 1	5.23e − 1
b ($g^{-\lambda-1}$ $cm^{3\lambda+2}$ $eV^{-\mu}$)	5.0e + 7	5.8824e + 10
μ	−2.0	−4.2
λ	0.3	0.8

mean-free path. From the parameter values in Table 1, the multiplier b in (25) is l_*^{-1} and the respective exponents for temperature and density in (25) are also easy to deduce. We further assume that the Planck mean opacity is roughly 5–10 times larger than the Rosseland mean opacity [40], and we use the approximation

$$\kappa_{\mathrm{P}}(T_{\mathrm{M}}, \rho) = 5\kappa_{\mathrm{R}}(T_{\mathrm{M}}, \rho). \tag{26}$$

4.1. Closed system

Our first model problem simulates the diffusion of radiation into a system in which there are reflecting boundaries. Since total energy is always conserved and all fluxes at the boundaries are zero, the steady-state temperature for the system can easily be computed given

$$aT_{\mathrm{steady}}^4 + \mathrm{EOS}(T_{\mathrm{steady}}) = \sum (E_{\mathrm{R}}(t_0) + E_{\mathrm{M}}(t_0)). \tag{27}$$

Besides being physically interesting, the closed system problem tells us in a simple and direct way the degree to which energy is conserved in the code and, consequently, to what level the sensitivities can be believed. It does no good, for example, to examine sensitivities to one part in 1000 if the code conserves energy to one part in 100; the sensitivities are then merely reflecting the lack of energy conservation. For the closed system test problems in Section 5, the relative error in the total energy at steady state is less than 10^{-9} in magnitude. This tight energy conservation gives us confidence that the sensitivities quoted in this paper are indeed due to physics and not numerics.

The radiation diffusion model is solved in the domain $0 \leqslant x \leqslant 0.1$ cm, $0 \leqslant y, z \leqslant 1$ cm with homogeneous Neumann boundary conditions on all of the faces. For initial conditions, $E_{\mathrm{R}} = aT_{\mathrm{R},0}^4$ and $E_{\mathrm{M}} = \mathrm{EOS}(T_{\mathrm{M},0})$ where

$$T_{\mathrm{R},0} = 1000 \text{ eV}, \quad 0.04 \leqslant x \leqslant 0.06 \text{ cm}, \text{ otherwise } 200 \text{ eV}, \tag{28}$$

$$T_{\mathrm{M},0} = 200 \text{ eV}, \quad 0 \leqslant x \leqslant 0.1 \text{ cm}. \tag{29}$$

The spatial grid was uniform and consisted of $50 \times 1 \times 1$ gridpoints. Before we continue, a comment is in order concerning the regime of applicability of the Basko analytic form of the opacity [22]. Technically, our test problems encounter temperature regimes outside of the range of validity. It must be remembered, however, that we are not trying to simulate an actual physical experiment, but rather we are merely using it as a reasonable representation of the opacity so as to elucidate the effects of strong parameter nonlinearity on sensitivity.

4.2. Marshak wave

Our second test problem is the one-dimensional Marshak wave. The radiation diffusion model is solved in the domain $0 \leqslant x \leqslant 0.1$ cm, $0 \leqslant y, z \leqslant 1$ cm with Dirichlet boundary conditions of $T_R = 300$ eV at $x = 0$ cm and $T_R = 30$ eV at $x = 0.1$ cm and homogeneous Neumann boundary conditions on the other faces. The initial conditions in the interior were $T_{R,0} = T_{M,0} = 30$ eV. The spatial grid was uniform and consisted of $50 \times 1 \times 1$ gridpoints.

5. Numerical results

The purpose of this section is to demonstrate our sensitivity analysis technique as applied to the model problems described above. In addition to descriptions of solution and sensitivity behavior, surface and line plots are included to enhance our understanding of the radiation diffusion process. Our first set of examples simulates radiation diffusion in the closed system test problem. In particular, we first present a detailed analysis for aluminum and its sensitivity to the temperature exponent μ. This extended analysis is helpful as a basis for comparison when other materials or sensitivity parameters are considered. The second set of examples is for the Marshak wave problem, and we also begin with the results for aluminum and μ. Lastly, the cost of computing solutions and sensitivities for the test problems is tabulated and we explain the reasons for the differences in total time to solve the problem.

5.1. Closed system

Our first closed system example is a detailed study of radiation diffusion through a slab of aluminum. Initial conditions are given in (28), (29). The surface plots in Fig. 1 show the radiation and material temperatures as they vary in time and along the x-axis in space. The process of material energy transfer is faster and occurs on a shorter time scale than the one for energy diffusion. To adequately capture the details of these processes, a logarithmic scale is used for the axis in time. During the first 10^{-9} μs, the peak value for radiation temperature decreases and the square-wave profile broadens slightly. The material temperature, however, has a more noticeable change as the loss of radiation temperature leads to an increase in the material temperature. This initial increase is governed by the material energy Eq. (2) and partly depends on the temperature difference $a(T_M^4 - T_R^4)$. The rate of increase also depends on and is slightly damped by the Planck mean opacity $\kappa_P(T_M, \rho)$, which decreases as the material temperature increases. These considerations also help account for the rate of decrease in the peak radiation temperature since the right-hand side of (2) appears as a negative source term in the radiation energy Eq. (1). The critical period between 10^{-9} and 10^{-6} μs is when the radiation and material temperatures couple rapidly. The peak radiation temperature drops below 1000 eV, and the material temperature peaks at 245 eV. Between 10^{-6} and 10^{-3} μs, radiation and material temperatures are nearly in equilibrium and they begin to diffuse throughout the rest of the spatial domain. The rate of diffusion is primarily influenced by the Rosseland mean opacity $\kappa_R(T_R, \rho)$. The diffusion process behaves like a Marshak wave centered around 0.05 cm with wavefronts that simultaneously move toward the left and right boundaries as the height of the wave falls. Between 10^{-3} and 0.1 μs, the radiation and material temperatures are essentially in equilibrium except the wavefront for radiation temperature slightly leads that for material temperature. Temperatures range within $[200, 240]$ eV and eventually approach the common steady state temperature of 209.4 eV after about 0.4 μs. For comparison and more detail, we also compute and plot solutions for radiation and material temperatures as they vary in time at $x = 0.05$ cm; see Fig. 2. The middle line plots correspond to temperatures computed using the nominal value for the temperature exponent, $\mu = -2.0$. The other line plots correspond to solutions

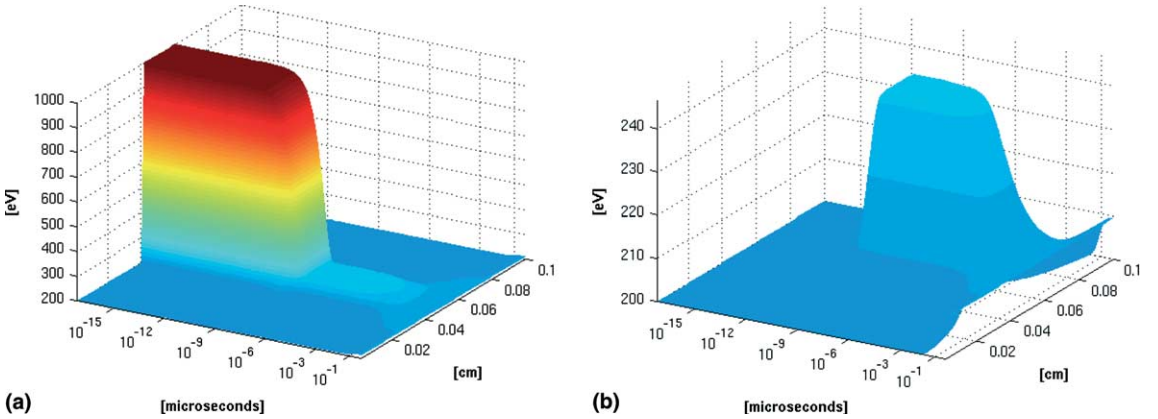

Fig. 1. Radiation and material temperatures for 1D radiation diffusion through aluminum shown as surface plots across time and space for the closed system model problem. (a) Radiation temperature for aluminum. (b) Material temperature for aluminum.

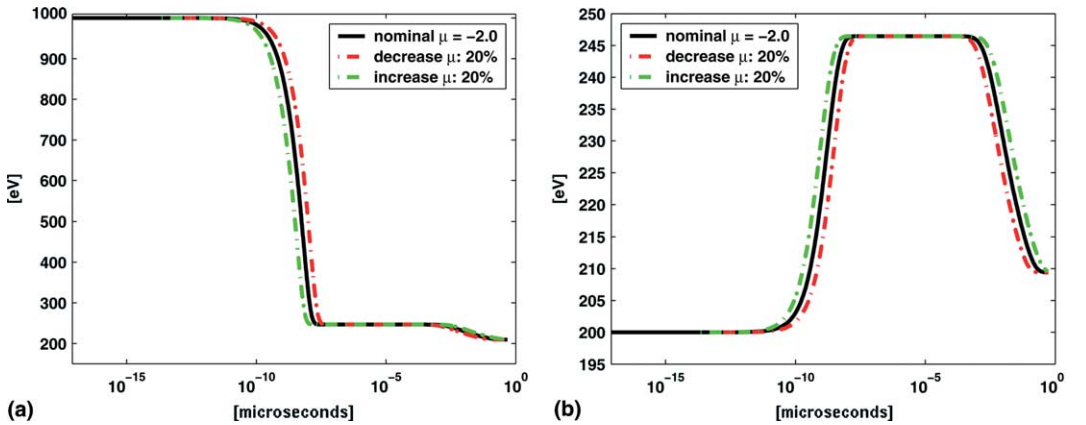

Fig. 2. Radiation and material temperatures at $x = 0.05$ cm for radiation diffusion through aluminum. Solutions are computed for three different values for the temperature exponent μ. (a) Radiation temperature for aluminum. (b) Material temperature for aluminum.

computed when μ is increased or decreased by 20%, and show that the nominal solution is affected by the value of μ.

In general, how sensitive is the above simulation to changes in μ or the other nominal values of the mean opacity parameters? The change in the nominal solutions can be estimated based on a rearrangement of the first-order Taylor series (20), (21). At each time step, the change in the nominal solutions is proportional to the scaled sensitivities, and the proportionality factor is the relative change in the parameter. For example, the surface plots in Fig. 3 show the scaled sensitivities with respect to the temperature exponent μ. The time, location, and nonzero values indicate when, where, and to what extent the nominal solution is predicted to change. Physically, a positive relative change in μ increases the mean opacities so that the larger Planck opacity accelerates the rate at which the radiation and material temperatures couple and the larger Rosseland opacity impedes the rate at which the coupled temperatures diffuse before reaching steady state. This information is revealed by the scaled sensitivities though some skill of interpretation is required. For example, it is important to notice that the upward sensitivity spike in Fig. 3(b) occurs slightly earlier in time than the material temperature rise in the nominal solution. This means the material temperature will

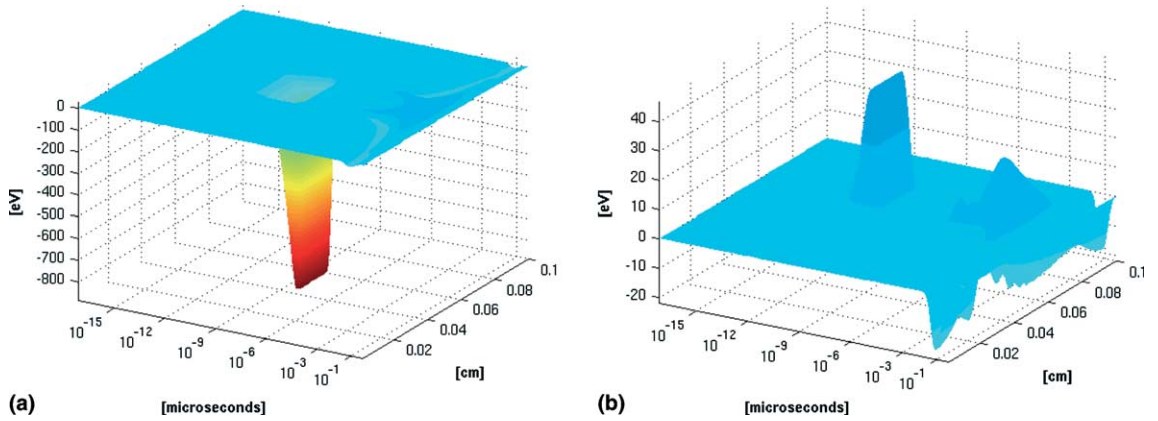

Fig. 3. Scaled sensitivity with respect to temperature exponent μ for 1D radiation diffusion through aluminum shown as surface plots across time and space for the closed system model problem. (a) Scaled sensitivity for radiation temperature in aluminum. (b) Scaled sensitivity for material temperature in aluminum.

increase earlier in time and in proportion to the relative increase in μ. Similarly, the negative sensitivity values corresponding to the downward spike in Fig. 3(a) predicts sharply reduced values for the nominal radiation temperature. Those lower temperatures correspond to the radiation temperature dropping sooner in time as it reaches equilibrium with the material temperature. After 10^{-6} μs, the later scaled sensitivity values are the same in both surface plots. As the radiation and material temperatures are essentially in equilibrium, they become equally sensitive to the same parameter. The elevated values after 10^{-3} μs indicate that the nominal temperatures are proportionally higher and do not fall as rapidly to steady state. Lastly, note that the sensitivity to the Planck and Rosseland mean opacities are decoupled in time. The downward and upward spikes that occur earlier in time are essentially the scaled sensitivities with respect to the temperature exponent μ in the Planck mean opacity. The identical sensitivities that occur later reveal the scaled sensitivities with respect to the temperature exponent in the Rosseland mean opacity.

We next consider the case in which beryllium is used for this model problem. Beryllium is less opaque than aluminum. In this case, the energy transfer governed by the Planck opacity is less rapid and more time is needed for temperatures to couple. Note that in Fig. 4, the radiation and material temperatures have the same, initial square-wave and flat profiles; however, the temperature coupling is somewhat delayed until about 10^{-6} μs. The peak material temperature is 248.3 eV, and the steady-state temperature of 215.7 eV is reached after about 0.006 μs. It is also evident that the coupling and diffusion processes do not occur in separate phases. The broadened face for radiation temperature indicates that its temperature is diffusing even as it falls. The material temperature also diffuses toward the boundaries as its peak value is attained. This overlap of processes is also revealed in the scaled sensitivity plots in Fig. 5. The radiation temperature sensitivity shows that the downward spike has diffused to the boundary. The material temperature sensitivity shows that the upward spike due to sensitivity in the Planck opacity is fused with the nonzero sensitivities that come from the Rosseland opacity.

5.2. Marshak wave

For the Marshak wave problem, the behavior of the radiation and material temperatures is roughly the same whether the material slab is composed of aluminum or beryllium. In the initial stage, the radiation temperature heats up more rapidly than the material temperature along the left boundary. As the radiation temperature reaches its peak value, it forms a wavefront that begins to move across to the right boundary.

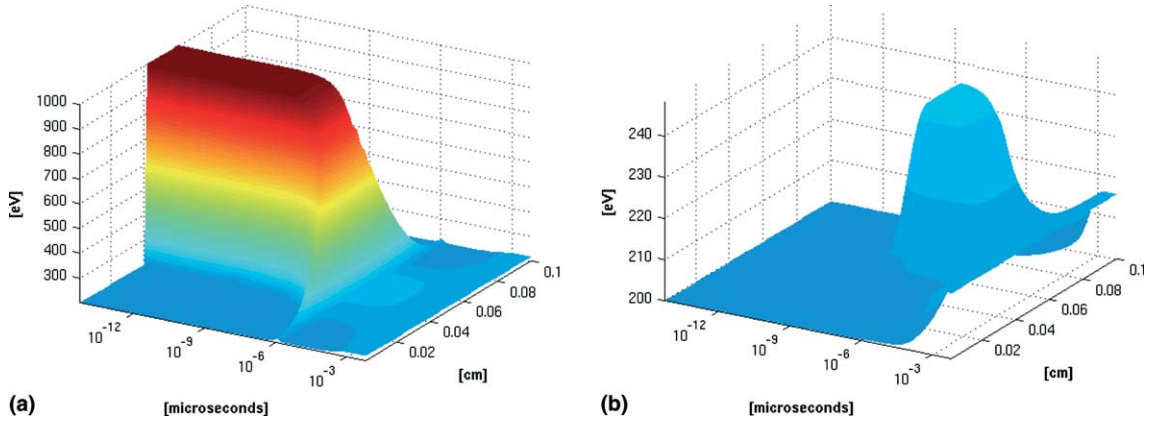

Fig. 4. Radiation and material temperatures for 1D radiation diffusion through beryllium shown as surface plots across time and space for the closed system model problem. (a) Radiation temperature for beryllium. (b) Material temperature for beryllium.

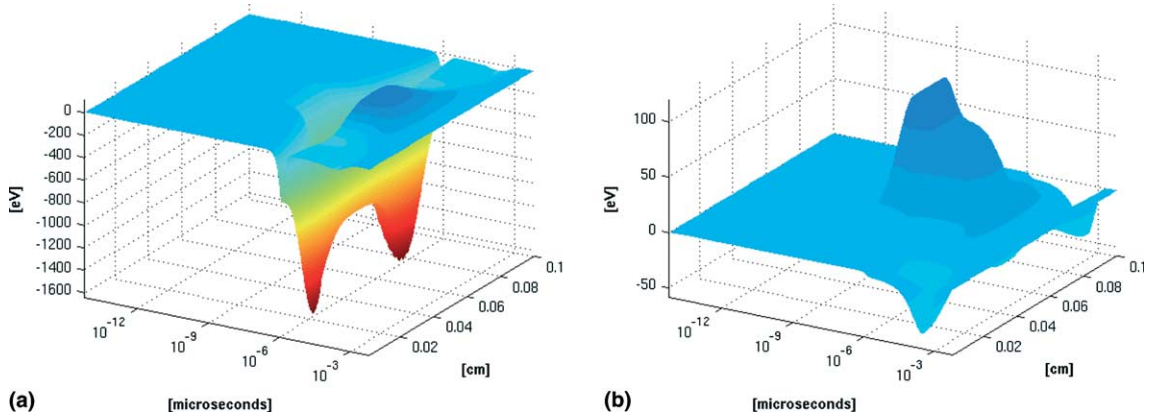

Fig. 5. Scaled sensitivity with respect to temperature exponent μ for 1D radiation diffusion through beryllium shown as surface plots across time and space for the closed system model problem. (a) Scaled sensitivity for radiation temperature in beryllium. (b) Scaled sensitivity for material temperature in beryllium.

Eventually, the material temperature reaches the same peak value along the left boundary and forms a wavefront that only slightly lags behind the radiation temperature wavefront. As in the closed system, the temperatures are nearly in equilibrium as the wavefronts move to the boundary; however, the Dirichlet boundary conditions ensure that the wave heights peak and do not fall as the wavefronts move across the domain. An example of the radiation wavefront for aluminum is given in Fig. 6(a).

The behavior of the sensitivities is also similar for the different materials and with respect to the opacity parameters μ, b, and λ. A typical example is given in Fig. 6(b), which shows the scaled sensitivity of the radiation temperature with respect to μ. Note that the sensitivities have sharp, negative peaks concentrated around the wavefront. As with the closed system, the negative sensitivity values predict sharply reduced values for the nominal radiation temperature given a positive relative change in μ. Those lower temperatures correspond to the radiation temperature lagging behind the nominal temperatures as the wavefront tries to diffuse through a more opaque material.

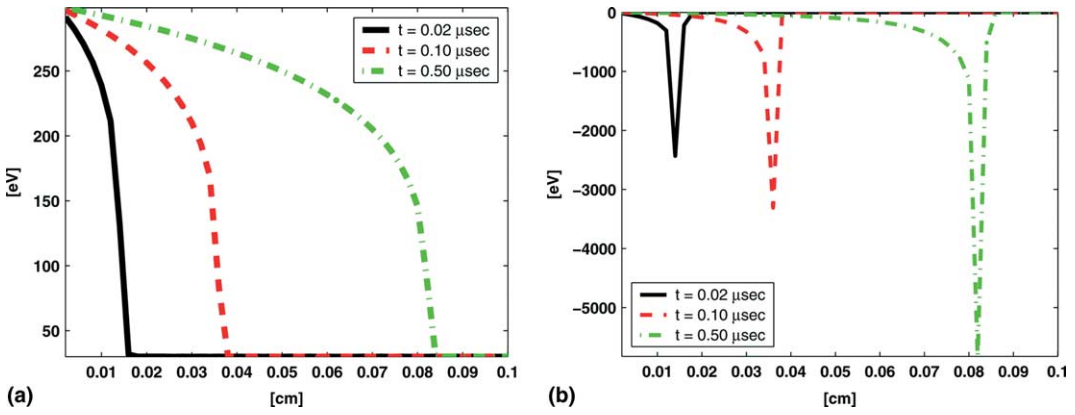

Fig. 6. Radiation temperature and its scaled sensitivity with respect to the temperature exponent μ for 1D radiation diffusion through aluminum for the Marshak wave model problem. (a) Radiation temperature for aluminum. (b) Scaled sensitivity for radiation temperature in aluminum.

5.3. Run times

The run time cost of computing scaled sensitivities is relatively inexpensive. Tables 2 and 3 show the run time and solver performance for computing the radiation diffusion solution and its scaled sensitivity with respect to zero, one, or all three parameters for the model problems. The key question is: how much additional run time is required in computing sensitivity information? In pairing each material and model problem, the tables show that the total number of time steps (NST) is approximately the same within each pairing and that this statistic only varies slightly when sensitivities are computed. The significant point for beryllium is that the average number of Newton iterations per timestep (NNI) is roughly 1.2 whether zero, one, or three scaled sensitivities are computed. In each Newton iteration, $1 + m$ linear systems are solved where m is the number of scaled sensitivities to be computed. The average number of linear iterations (NLI) of GMRES per Newton iteration roughly increases by a factor of $1 + m$ and indicates that solving for Newton updates to energies or sensitivities is of comparable difficulty. For the aluminum test results, the average number of Newton iterations increases by a factor of 1.5–3 when computing scaled sensitivity with respect to a single parameter, and this increased work in converging Newton iterations roughly quadruples the run time. Despite this fourfold increase for a sensitivity computation, we note only a modest increase when additional sensitivities are computed (e.g., all three). So, although individual sensitivity computations may more than double the run time of the original simulation, the cost-effectiveness can improve when several sensitivities are computed together. Lastly, Table 4 shows some results for computing all three scaled sensitivities and/or the solution for larger problem sizes for the closed system problem. The run times

Table 2
Aluminum solver statistics: solution and scaled sensitivities

	Closed system				Marshak wave			
	Time (s)	Total NST	Avg NNI	Avg NLI	Time (s)	Total NST	Avg NNI	Avg NLI
None	2.63	456	1.14	2.57	10.36	1311	1.10	4.33
μ	11.08	453	2.41	4.80	55.60	1335	3.02	7.66
b	10.02	458	2.13	4.85	52.98	1319	2.99	7.38
λ	8.15	462	1.63	5.26	50.56	1319	2.94	7.09
μ, b, λ	25.25	458	2.33	11.47	133.09	1335	3.02	18.74

Table 3
Beryllium solver statistics: solution and scaled sensitivities

	Closed system				Marshak wave			
	Time (s)	Total NST	Avg NNI	Avg NLI	Time (s)	Total NST	Avg NNI	Avg NLI
None	6.58	791	1.20	4.05	20.60	1863	1.18	5.96
μ	14.48	790	1.21	8.48	43.68	1912	1.19	11.68
b	12.92	781	1.17	7.75	40.00	1911	1.17	10.68
λ	12.53	781	1.17	7.45	38.62	1894	1.16	10.41
μ, b, λ	27.62	790	1.18	15.84	79.41	1872	1.18	20.76

Table 4
Closed system results for larger problem sizes: run time in seconds for solution and scaled sensitivities

	Al			Be		
	$100 \times 1 \times 1$	$250 \times 1 \times 1$	$500 \times 1 \times 1$	$100 \times 1 \times 1$	$250 \times 1 \times 1$	$500 \times 1 \times 1$
None	5.16	13.46	29.90	21.73	120.50	466.13
μ, b, λ	50.93	140.09	320.77	95.76	550.94	3270.00

for aluminum are consistent with our earlier observations: computing all three scaled sensitivities increases the run time roughly by a factor of 10 relative to solving the simulation by itself. The run time results for beryllium are also favorable. The relative increase in run time ranges only by a factor of 4–7 for increased problem sizes.

6. Sensitivity applications

In this section, we demonstrate the usefulness and versatility of sensitivity computations as applied to the analysis of radiation diffusion models.

6.1. Model evaluation

One application of sensitivity analysis focuses on the sensitivity of model behavior due to perturbations in the nominal parameter values. The objective of such analysis is to identify the parameters most influential in affecting simulation results. Given that each nominal parameter value is typically chosen from a range of values, our confidence in simulation results can be enhanced by narrowing the range of uncertainty for the most influential parameters. This range can be narrowed, for example, by taking additional measurements that yield a more accurate determination of the parameter range. A complementary objective is to identify parameters for which simulation results are not sensitive. By identifying the most insensitive parameters, it may be possible to create a reduced model with fewer equations and/or parameters but this topic is beyond the scope of this paper.

The relative ranking of most to least influential parameters can be obtained by examining the magnitude of the simulation response to relative perturbations in the mean opacity parameters. In particular, the scaled sensitivities of largest magnitude (positive or negative) can be plotted at each gridpoint for each parameter for all time. An example is given in Fig. 7 for the radiation and material temperatures of aluminum in the closed system. The nested line plots in Fig. 7(a) signify that the radiation temperature experiences the largest amount of change due to relative perturbations in μ, b, and λ respectively. Fig. 7(b) shows that this nesting and strict ranking also holds for the material temperature. Analogous plots for the

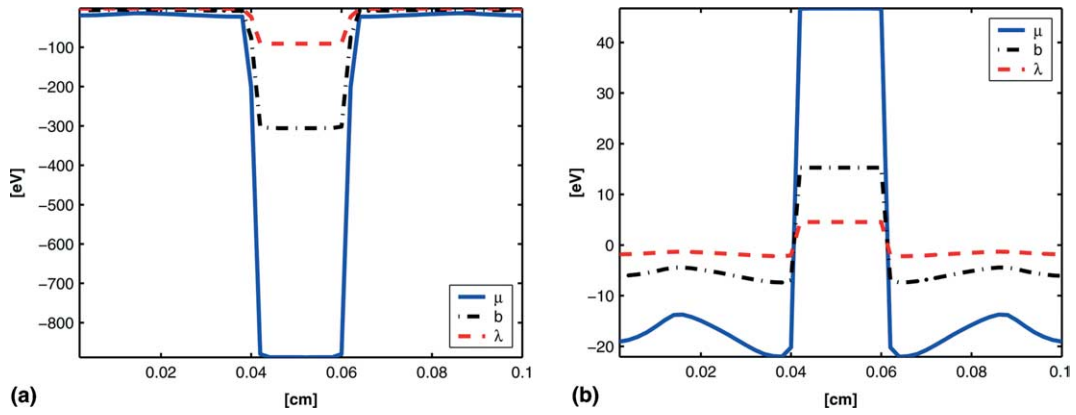

Fig. 7. Maximum magnitude of scaled sensitivities in time for radiation diffusion through aluminum for closed system model problem. (a) Maximum scaled sensitivity for T_R. (b) Maximum scaled sensitivity for T_M.

other three pairings of test problems and materials yield the same ranking order. Therefore, we conclude that uncertainty in the temperature exponent μ is most significant in affecting the uncertainty in the simulation results.

Another useful technique for this example is to visualize sensitivities and the simulation solution together. If we consider normalized sensitivities, we can assess the relative changes in the simulation solution versus relative perturbations in the mean opacity parameters. The surface plots in Fig. 8 show the simulation solution for aluminum in the closed system, so they are the same as in Fig. 1. Note, however, that the surface colors in Fig. 8 correspond to the normalized sensitivity with respect to μ. The magnitudes for these normalized sensitivities are given by the different colorbars in Fig. 8. For a relative perturbation in μ, the relative changes in the radiation and material temperatures are proportional to the value of their corresponding normalized sensitivities. Fig. 8(a) and (b) show that the relative changes are the greatest as the two temperatures come into equilibrium at around 10^{-9} μs. The greater portion of both surface plots, however, show that the simulation solution has zero sensitivity to initial perturbations in the parameters. It is mainly

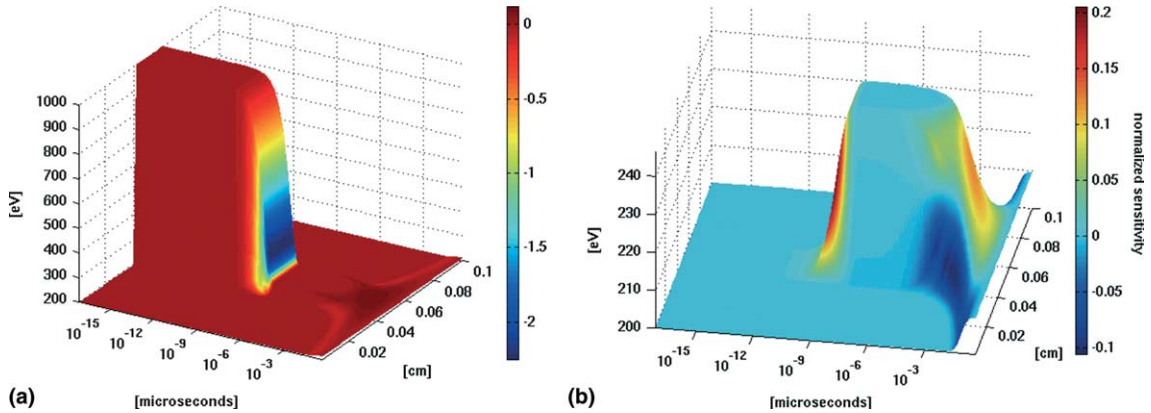

Fig. 8. Radiation and material temperature for radiation diffusion through aluminum in the closed system. Surface colors correspond to normalized sensitivity with respect to temperature exponent μ. (a) Radiation temperature. (b) Material temperature.

when temperature coupling or diffusion is active that the simulation solution has increased responsiveness, which the overlaid normalized sensitivities help identify and quantify.

6.2. Experimental design

With the advent of new technology, real time, in situ diagnostics are a distinct possibility. An example would be advanced sensors that might measure the temperature and density inside a material that is being shocked and heated. Such dynamic information would provide a wealth of data concerning equation of state and opacity. Sensitivity analysis is a tool that can guide experimental design and diagnostics in such a way as to make maximum use of the experiment. Going further, sensitivity analysis can tell us where and when the maximum sensitivity occurs and in what variable. For example, in the Marshak wave problem, the sensitivity calculations in Fig. 6(b) show that the arrival time of the radiation temperature front is a very sensitive indicator of opacity variations. An experimentalist, therefore, might choose to measure the arrival time of the radiation temperature and thereby obtain an accurate determination of an opacity parameter [41].

6.3. Uncertainty quantification

A third application of sensitivity analysis is in bounding the amount of uncertainty in the simulation results in terms of the amount of uncertainty in the model parameters. In some cases, many parameter measurements are available, and probability density functions (pdfs) or at least the variances for the parameters are known. In such instances, particular sensitivity techniques can be used to determine a first-order estimate of the pdfs or variances for the simulation results. If we assume a uniform parameter distribution or simply that the parameters lie in a fixed range, the scaled sensitivities can also be used to bound the range for the simulation results.

We can demonstrate this uncertainty quantification for the closed system test problem for aluminum based on the nominal solution, its scaled sensitivity with respect to μ, and (20), (21). In Fig. 9(a), the middle line plot shows the radiation temperature as it varies in time and goes to steady state at $x = 0.05$ cm. By assuming that the nominal parameter $\mu = -2.0$ varies by at most 20%, we are able to bound the uncertainty of the radiation temperature based on its scaled sensitivity. Similarly, Fig. 9(b) bounds the uncertainty in

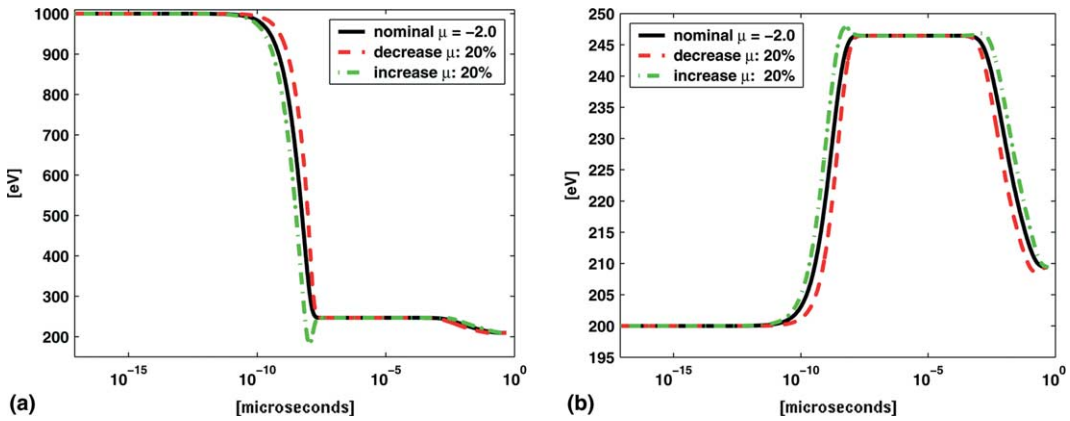

Fig. 9. Radiation and material temperatures, with bounds estimated for ±20% uncertainty in the temperature exponent μ for radiation diffusion through aluminum in the closed system. (a) Radiation temperature. (b) Material temperature.

the material temperature due to the uncertainty in μ. Note that the simulation uncertainty is large at two separate times: during the process of material energy transfer, and during the diffusion process. We also find that these bounds are good first-order predictions of the solutions computed when μ is changed by $\pm 20\%$. In particular, the solutions plotted in Fig. 2 are in good agreement with those predicted in Fig. 9. The most notable difference is the slight undershoot and overshoot in the predicted radiation and material temperatures, respectively. The predictions are more accurate, however, if the relative change in the nominal value is more modest or a less influential parameter (i.e., b or λ) is studied.

7. Conclusions

We have developed and introduced new sensitivity-based methods for the analysis of radiation diffusion problems. The proposed techniques are applied to simplified but physically realistic models of radiation diffusion and material opacity. The sensitivity equations are derived by differentiating the radiation and material energy equations with the respect to the mean opacity parameters. Sensitivities are computed by solving the derived equations in tandem with the simulation, rather than using a finite difference technique based on running the simulation with two different values of the same parameter. Our main contribution was to address several important questions related to the simulation results and their sensitivity to the mean opacity parameters. These questions centered on the effects of changes in the opacity parameter values, the cost of computing sensitivities, the identification of the most and least influential parameters, and the use of sensitivities for experimental design and uncertainty quantification. The significance of our work is that we can answer these questions based on the sensitivity analysis techniques that we have developed.

One of the main conclusions of this work is that obtaining solution sensitivities is not an expensive computation compared to the run time cost of computing the solution by itself – the ratio ranged between 2–14 depending on the test problem, material, and parameters selected. The second finding is that computing sensitivities is an effective technique for obtaining valuable information about the simulation. A coarse intuition of model behavior and sensitivities can be developed from a general understanding of the model problem and the underlying physics. As demonstrated, a study of scaled sensitivities can provide supplemental, quantitative details that may be difficult to deduce from first principles – such as the location and duration for when sensitivities are relatively large or small. Lastly, we conclude that sensitivity-based techniques for uncertainty quantification are effective tools for improving user confidence in simulation results. We demonstrated that sensitivities can be used to give a first-order estimate of the uncertainty in simulation results in terms of the uncertainty in each parameter value. Moreover, experimental design techniques are one means of determining where additional experimental measurements may be needed to tighten the bounds on parameter uncertainties. We also discussed that with recently developed software (Section 3.5), existing codes can be reasonably modified to compute sensitivities with this approach. Future work in this area will include the application of these sensitivity-based techniques to other radiation diffusion and parameter-dependent scientific problems.

Acknowledgements

The authors wish to thank Peter Brown for numerous discussions on sensitivity analysis techniques and software and Keith Grant for the initial port of SensPVODE to our diffusion code. The authors also acknowledge Rachel Knopp for initial comparisons of our sensitivity techniques with finite difference methods. This work was performed under the auspices of the U.S. DOE by LLNL under contract No. W-7405-Eng-48.

References

[1] J.D. Lindl, Inertial Confinement Fusion: The Quest for Ignition and Energy Gain Using Indirect Drive, Springer, New York, 1998.
[2] J.M. Stone, D. Mihalas, M.L. Norman, ZEUS-2D: A radiation magnetohydrodynamics code for astrophysical flows in 2 space dimensions: 3. The radiation hydrodynamic algorithms and tests, Astrophys. J. Suppl. 80 (1992) 819–845.
[3] R.L. Bowers, J.R. Wilson, Numerical Modeling in Applied Physics and Astrophysics, Jones and Bartlett, Boston, 1991.
[4] G. Tsakiris, K. Eidmann, An approximate method for calculating Planck and Rosseland mean opacities in hot, dense plasmas, J. Quantum Spectrosc. Radiat. Transfer 38 (5) (1987) 353–368.
[5] F. Rogers, C. Iglesias, Radiative atomic Rosseland mean opacity tables, Astrophys. J. Suppl. Ser. 79 (2) (1992) 507–568.
[6] F. Rogers, A. Nayfonov, Updated and expanded OPAL equation-of-state tables: Implications for helioseismology Part 1, Astrophys. J. 576 (2) (2002) 1064–1074.
[7] P.N. Brown, K.E. Grant, C.S. Woodward, On the Calculation of Uncertainties for 3D time-dependent neutral particle transport, Center for Applied Scientific Computing UCRL-JC-146186, Lawrence Livermore National Laboratory, Livermore, CA, 2001.
[8] C.S. Woodward, K.E. Grant, R. Maxwell, Applications of sensitivity analysis to uncertainty quantification for variably saturated flow, in: S.M. Hassanizadeh, R.J. Schotting, W.G. Gray, G.F. Pinder (Eds.), Computational Methods in Water Resources, vol. 1, Elsevier, Amsterdam, 2002, pp. 73–80.
[9] K.J. Dowding, B.F. Blackwell, Sensitivity analysis for nonlinear heat conduction, J. Heat Transfer 123 (2001) 1–10.
[10] M. Tocci, Sensitivity analysis of large-scale time dependent PDEs, Appl. Numer. Math. 37 (1-2) (2001) 109–125.
[11] W. Feehery, J. Tolsma, P. Barton, Efficient sensitivity analysis of large-scale differential-algebraic systems, Appl. Numer. Math. 25 (1) (1997) 41–54.
[12] P.N. Brown, B. Chang, F. Graziani, C.S. Woodward, Implicit solution of large-scale radiation material-energy transfer problems, in: D.R. Kincaid, A.C. Elster (Eds.), Iterative Methods in Scientific Computation IV, Series in Computational and Applied Mathematics, vol. 5, International Association for Mathematics and Computers in Simulations, New Brunswick, NJ, 1999, pp. 343–356.
[13] V.A. Mousseau, D.A. Knoll, W.J. Rider, Physics-based preconditioning and the Newton–Krylov method for non-equilibrium radiation diffusion, J. Comput. Phys. 160 (2000) 743–765.
[14] P.N. Brown, C.S. Woodward, Preconditioning strategies for fully implicit radiation diffusion with material-energy transfer, SIAM J. Sci. Comput. 23 (2) (2001) 499–516.
[15] V.A. Mousseau, D.A. Knoll, New physics-based preconditioning of implicit methods for non-equilibrium radiation diffusion, J. Comput. Phys. 190 (1) (2003) 42–51.
[16] D.J. Mavriplis, Multigrid approaches to non-linear diffusion problems on unstructured meshes, Numer. Linear Algebra Appl. 8 (8) (2001) 499–512.
[17] L.H. Howell, J.A. Greenough, Radiation diffusion for multi-fluid Eulerian hydrodynamics with adaptive mesh refinement, J. Comput. Phys. 184 (2003) 58–78.
[18] D.A. Knoll, W.J. Rider, G.L. Olson, An efficient nonlinear solution method for non-equilibrium radiation diffusion, J. Quantum Spectrosc. Radiat. Transfer 63 (1999) 15–29.
[19] D.A. Knoll, W.J. Rider, G.L. Olson, Nonlinear convergence, accuracy, and time step control in nonequilibrium radiation diffusion, J. Quantum Spectrosc. Radiat. Transfer 70 (1) (2001) 25–36.
[20] P.N. Brown, F. Graziani, I. Otero, C.S. Woodward, Implicit solution of large-scale radiation diffusion problems, Center for Applied Scientific Computing UCRL-JC-141881, Lawrence Livermore National Laboratory, Livermore, CA, in: Proceedings of Nuclear Explosives Code Developers' Collaborations 2000, Oakland, CA, Oct. 2000 (Jan. 2001).
[21] G.C. Pomraning, The Equations of Radiation Hydrodynamics, Pergamon, New York, 1973.
[22] M. Basko, A model for the conversion of ion-beam energy into thermal radiation, Phys. Fluids B 4 (11) (1992) 3753–3763.
[23] E. Mínguez, P. Martel, J. Gil, J. Rubiano, R. Rodríguez, Analytical opacity formulas for ICF elements, Fusion Eng. Design 60 (2002) 17–25.
[24] G.D. Byrne, A.C. Hindmarsh, PVODE, an ODE solver for parallel computers, Int. J. High Perf. Comput. Appl. 13 (1999) 354–365.
[25] P.N. Brown, G.D. Byrne, A.C. Hindmarsh, VODE: a variable-coefficient ODE solver, SIAM J. Sci. Statist. Comput. 10 (5) (1989) 1038–1051.
[26] K.R. Jackson, R. Sacks-Davis, An alternative implementation of variable step-size multistep formulas for stiff ODEs, ACM Trans. Math. Software 6 (1980) 295–318.
[27] P.N. Brown, A.C. Hindmarsh, Matrix-free methods for stiff systems of ODEs, SIAM J. Numer. Anal. 23 (1986) 610–638.
[28] Y. Saad, M.H. Schultz, GMRES: a generalized minimal residual algorithm for solving nonsymmetric linear systems, SIAM J. Sci. Statist. Comput. 7 (3) (1986) 856–869.
[29] W.F. Briggs, V.E. Henson, S.F. McCormick, A Multigrid Tutorial, second ed., SIAM, Philadelphia, PA, 2000.
[30] S.L. Lee, A.C. Hindmarsh, P.N. Brown, User documentation for SensPVODE, a variant of PVODE for sensitivity analysis, Tech. Rep. UCRL-MA-140211, Lawrence Livermore National Laboratory, 2000.

[31] T. Maly, L. Petzold, Numerical methods and software for sensitivity analysis of differential-algebraic systems, Appl. Numer. Math. 20 (1997) 57–79.
[32] C. Bischof, L. Roh, ADIC – an extensible automatic differentiation tool for ANSI-C, Software – Practice & Experience 27 (12) (1997) 1427–1456.
[33] S.L. Lee, P.D. Hovland, Sensitivity analysis using parallel ODE solvers and automatic differentiation in C: sensPVODE and ADIC, in: G. Corliss, C. Faure, A. Griewank, L. Hascoet, U. Naumann (Eds.), Automatic Differentiation of Algorithms: From Simulation to Optimization, Springer, New York, 2001, pp. 223–229.
[34] A.C. Hindmarsh, R. Serban, User Documentation for CVODES, an ODE solver with sensitivity analysis capabilities, Tech. Rep. UCRL-MA-148813, Lawrence Livermore National Laboratory, July 2002.
[35] K. Radhakrishnan, A.C. Hindmarsh, Description and Use of LSODE, the Livermore solver for ordinary differential equations, Tech. Rep. UCRL-ID-113855, Lawrence Livermore National Laboratory, Livermore, CA, 1993.
[36] A.C. Hindmarsh, P.N. Brown, K.E. Grant, S.L. Lee, R. Serban, D.E. Shumaker, C.S. Woodward, SUNDIALS: Suite of nonlinear and differential/algebraic equation solvers, ACM Trans. Math. Software, 2003, submitted. Available as Livermore National Laboratory Technical Report UCRL-JP-200037.
[37] S. Li, L.R. Petzold, Design of New DASPK for sensitivity analysis, Tech. Rep. 1999-28, University of California at Santa Barbara, May 1999.
[38] K.E. Brenan, S.L. Campbell, L.R. Petzold, Numerical Solution of Initial-Value Problems in Differential-Algebraic Equations, SIAM, Philadelphia, PA, 1996.
[39] C. Bischof, A. Carle, P. Khademi, A. Mauer, ADIFOR 2.0: Automatic differentiation of Fortran 77 programs, IEEE Comput. Sci. Eng. 3 (1996) 18–32.
[40] J. Bond, K. Watson, J. Welch, Atomic theory of gas dynamics, Addison-Wesley, Reading, MA, 1965.
[41] H.R. Griem, Principles of Plasma Spectroscopy, Cambridge University Press, New York, 1997.